

Obstacle Avoidance Control of Humanoid Robot Arm through Tactile Interaction

Dzmitry Tsetserukou, Naoki Kawakami, Susumu Tachi

University of Tokyo, Japan, dima_teterukov@ipc.i.u-tokyo.ac.jp, {kawakami,tachi}@star.t.u-tokyo.ac.jp

Abstract— In this paper we introduce a novel concept of obstacle avoidance through tactile interaction. The implementation of the approach was realized on humanoid robot arm with optical torque sensors distributed to each robot joint. When manipulator collides with an object, the control system enables to follow the object outline smoothly till robot reaches the target point. Such approach ensures not only safe obstacle avoidance but also acquisition of indispensable information about environment. The methods of object stiffness calculation, contact point estimation, and shape interpolation are detailed in the paper. The possible tasks of the robot with intelligent whole-arm obstacle avoidance control are summarized and illustrated in this work as well. The controllable compliance of robot arm joint can be extremely useful in a wide range of applications.

I. INTRODUCTION

Obstacle avoidance and motion planning are both necessary components for any robotic task. Obstacle avoidance refers to planning collision-free trajectories for robotic systems while motion planning refers to planning smooth motions.

Many efforts have been devoted to path planning in cluttered environment, but in most of approaches the exact world model is assumed and no sensors are utilized [1], [2]. When we consider the real indoor environments, known obstacles (e.g. chairs, tables, etc.) and unknown obstacles (persons approaching the robot, unmapped environment, etc.) change their location dynamically. Moreover, the object shape, speed and position can also alter in unpredictable way. Robot control system operating in unstructured dynamic environment must execute skilful manoeuvre that avoids a collision and directs the robot to its goal position. In order to provide the robot with detailed real-time environment view it is imperative to use sensor data.

The most effective solution of preventing collision is to endow the whole robot arm with the ability to safely interact and contact with environment in real time. Lumelsky [3] pioneered in the idea to cover manipulator with a sensitive skin capable of detecting nearby objects. An array of infrared proximity sensors delivers the information about obstacles obstructing arm motion to the control system. The algorithm of motion planner manoeuvres the robot arm avoiding impact [4]. Recently proposed sophisticated imaging systems, such as stereovision and laser scanning, presume usage of expensive detectors and complex signal processing techniques. They sense only narrow space around the robot body. The concept of sensor array composed of ultrasonic rangefinders and infrared detectors is described in [5]. Researchers are pursuing the goal of the development of a robust proximity sensor

system with application in mobile robotics, taking advantage of high performance/cost ratio of the components and low computational demands of the detection method.

Due to the specular nature of ultrasonic waves reflection, the only objects normally located to the sensor acoustic axis can be accurately detected. When it comes to infrared sensor, one of the most important problems is limited measuring performance. The amplitude from the infrared sensor largely depends on reflectivity of the object, and it changes with the target distance in non-linear manner. There is high possibility that proximity sensors fail to detect obstacle along the robot trajectory. In this case an immediate vicinity of the target can mislead robot control system invoking the abrupt change in the speed resulting in harm of the environment.

We argue that robot should be mainly controlled not to avoid the collision but rather to ensure tactile interaction with environment. The benefits of such interaction are obvious in nature. From the early childhood, humans touch objects to investigate the world and acquire a plenty of fundamental information about objects (shape, stiffness, texture, location, fixation, etc.). Conventional approaches to handle the interaction between a manipulator and environment are based on impedance control of a robot arm according to applied force vector measured at the manipulator wrist [6]. However, the rest parts of the robot body (forearm, elbow, upper arm, shoulder, and torso) are presenting significant danger not only to human being, but also to the robot structure itself. A fairly small work has been done on tactile interaction of the whole robot arm with environment.

Bauer [7] conducted very practical and useful research on exploration of the environment and accomplishment of pushing task by autonomous mobile robot. The idea underlying the algorithm is to identify free space, the object location, and object shape by several attempts made by the robot arm in order to pass obstacle through. It should be noted, however, that the proposed system cannot detect the contact point coordinates, requires time-consuming obstacle identification process, and, as authors reported, the exploration algorithm fails when several collisions occur simultaneously.

To cope with spatial uncertainty of unknown, unstructured environment we elaborated novel technique of obstacle avoidance through interaction. When the robot arm is obstructed by obstacle the controller directs the manipulator to the target point in such a way that robot arm surface follows the contour of the object.

II. ROBOT ARM AND SENSORY SYSTEM

The developed robot arm (Fig. 1(a)) has 4-DOF: Roll, Pitch, Yaw joints of a shoulder, and Pitch joint of an elbow. Such orthogonal disposition of the axes simplifies the installation of the torque sensors and motor drives into the joints, allowing thus avoidance of application of additional belt driven actuators. Coordinate systems based on Denavit-Hartenberg convention are represented in Fig. 2. The 8-DOF robot hand allows performing dexterous manipulations.

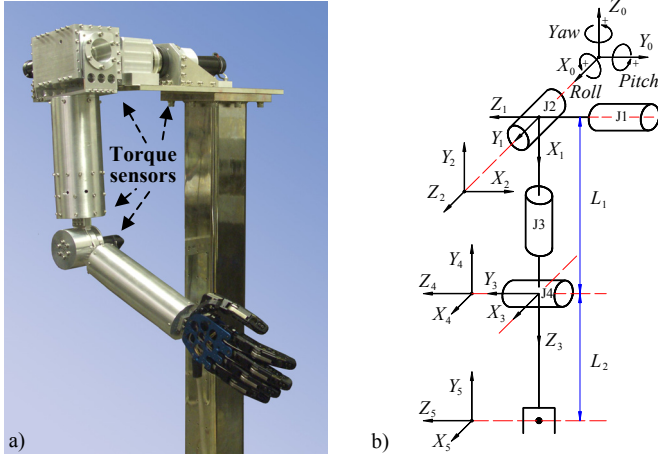


Fig. 1 Humanoid robot arm and coordinate system

Each robot joint is equipped with optical torque sensor directly connected to the output shaft of harmonic drive. We kept the arm proportions the same as in average height Japanese male, aged 25: upper arm length L_1 of 0.308 m; upper arm circumference of 0.251 m; forearm length L_2 of 0.241 m; forearm circumference of 0.189 m.

In order to facilitate the realization of torque measurement in each arm joint, we developed new optical torque sensors based on results presented in [8]. The novelty of our method is application of the ultra-small size photointerrupter (PI) RPI-121 as sensitive element to measure relative motion of sensor components. The dimensions of the PI (3.6 mm \times 2.6 mm \times 3.3 mm) and its weight of 0.05 g allow realization of compact design. The optical torque sensor is set between the driving shaft of the harmonic transmission and driven shaft of the joint (Fig. 2). When the load is applied to the robot joint, the magnitude of the output signal from the PI corresponds to the exerted load.

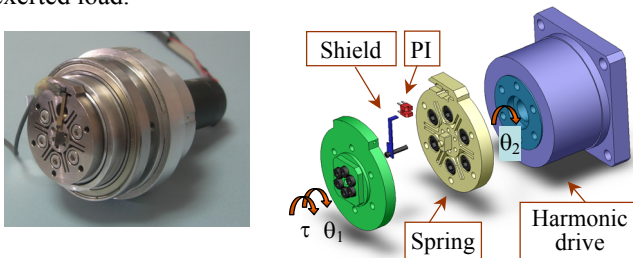


Fig. 2 Torque sensor of the elbow joint

The spring members attached to the first, second, and third/fourth joints were designed to measure torque of ± 12.5

Nm, ± 10.5 Nm, and ± 4.5 Nm respectively. Each sensor was calibrated by means of attachment of reference weights to the lever arm. Non-linearity of 2.5 % of Full Scale was calculated using maximum deviated value from the best-fit line.

The developed optical torque sensors have high dependability, good accuracy (even in electrically noisy environment), low price, compact sizes, and light weigh.

III. CONTACTING OBJECT PARAMETER IDENTIFICATION WITH TACTILE SENSING

A. Contact State Recognition

During the first stage of control the robot links rotate until one of them contacts the object. Below, the elaborated algorithm of contact detection is demonstrated.

In addition to contact force, torque sensors continuously measure the gravity and inertial load. As robot arm moves with low angular speed, the inertial load component can be disregarded. Let us consider gravity torque calculation in the case when robot arm performs only planar motion, and only the first and fourth joints operate (Fig. 3).

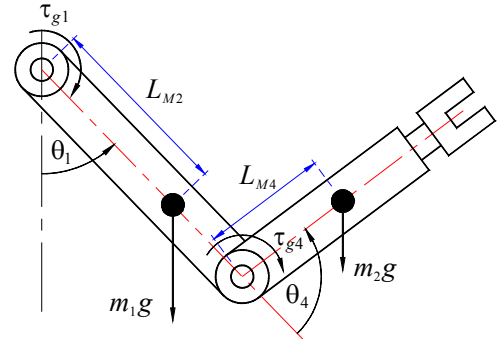


Fig. 3 Robot arm subjected to gravity loading

The Newton-Euler dynamics formulation was adopted to calculate reference value of the gravity torques. The gravity torques acting in the first τ_{g1} and fourth joints τ_{g4} are derived from:

$$\begin{aligned} \tau_{g1} &= m_2 g (L_{M4} \sin(\theta_1 + \theta_4) + L_2 \sin(\theta_1)) + m_1 g L_{M2} \sin(\theta_1) \\ \tau_{g4} &= m_2 g L_{M4} \sin(\theta_1 + \theta_4), \end{aligned} \quad (1)$$

where m_1 and m_2 are the point masses of the first and second link, respectively; L_{M2} and L_{M4} are the distances from the first and second link origins to the centers of mass, respectively.

The experiment with the fourth joint of the robot arm was conducted in order to measure the gravity torque (Fig. 4(a)) and to estimate the error by comparison with reference model (Fig. 4(b)).

As can be seen from Fig. 4, the pick values of the gravity torque estimation error arise at the start and stop stages of the joint rotation. The reason of this is high inertial loading that provokes the vibrations during acceleration and deceleration transient. This disturbance can be evaluated by using accelerometers and excluded from further consideration. Observing the measurement error plot, we can assign the relevant threshold that triggers control of constraint motion.

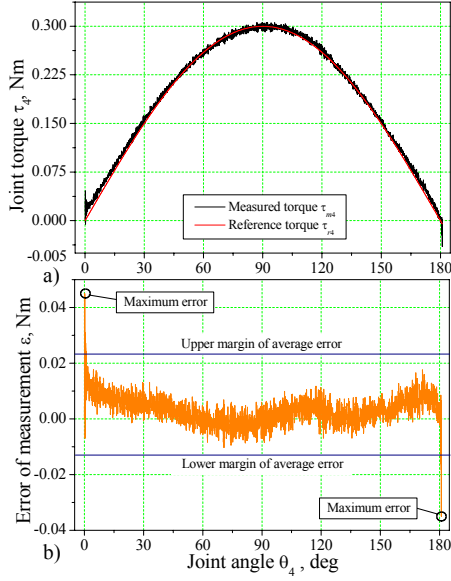


Fig. 4 Experimental results of gravity measurement

B. Estimation of Contacting Object Stiffness

During contact transition we can acquire information about collision danger of contacting object through its stiffness estimation. This can be done by establishing stiff contact through PD control of robot arm with high P-gain and setting the high threshold value. For the following experimental results the threshold was chosen as high as 0.05 Nm.

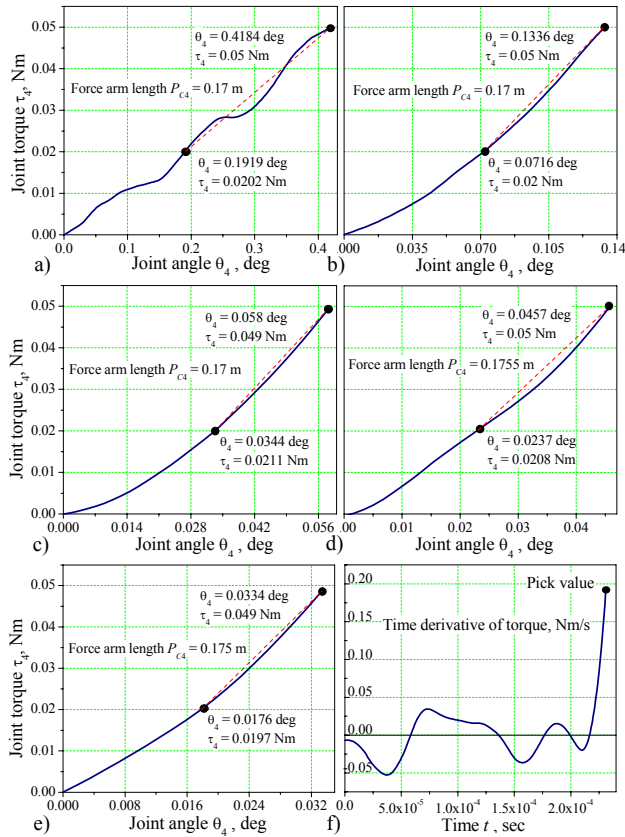


Fig. 5 Experimental results of stiffness estimation

The robot was commanded to follow the trajectory in free space with constant angular velocity. An object was placed on this path so that the second link would contact it. The joint torque was recorded for the fourth joint while contacting with object. The Fig. 5(a-e) shows experimental results when link comes into contact with objects having different stiffness varying from very low rate to very high, namely, piece of sponge, rubber sponge, rubber, chemical wood, and aluminum, respectively. The time derivative of torque during impact with aluminum plate is given in Fig. 5(f). It is apparent from the plots presented above that the stiffer object comes into contact with robot arm the smaller angle the joint rotates. Heterogeneous nature of sponge material explains highly non-linear behavior of stiffness curve (Fig. 5(a)).

The elastic deformation of the object and inherent compliance of the robot joints lead to rotation of robot arm by angle $\Delta\theta_i$ during contact transience (Fig. 6).

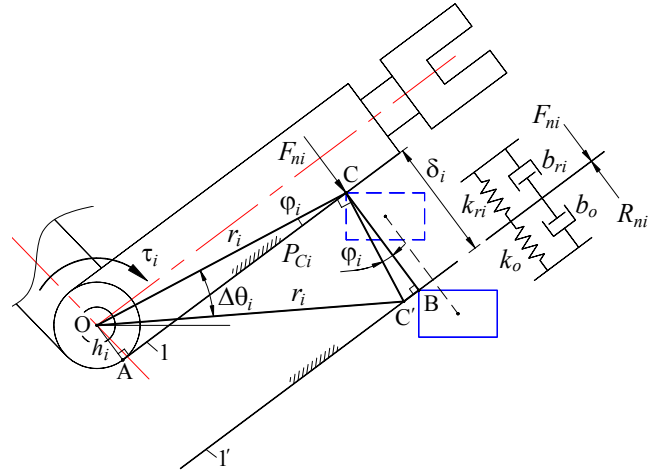


Fig. 6 The scheme for elastic deformation calculation

The distance, on which contact point C on the robot link surface 1 moves perpendicularly to the radius r_i under torque $\Delta\tau_i$, is equal to $r_i\Delta\theta_i$ (since the angle $\Delta\theta_i$ is small). The unknown angle φ_i can be found taking into account that $\angle C'CB = \angle OCA = \varphi_i$:

$$\varphi_i = \arctan\left(\frac{OA}{CA}\right) = \arctan\left(\frac{h_i}{P_{C_i}}\right), \quad (2)$$

where h_i equals half of the robot link thickness.

From the right triangle $\Delta CBC'$ the total elastic deformation is calculated as:

$$\delta_i = \Delta\theta_i r_i \cos(\varphi_i). \quad (3)$$

Radius of contact point trajectory r_i is found as $r_i = \sqrt{P_{C_i}^2 + h_i^2}$ through consideration of right triangle ΔCAO .

Now, we can easily solve for total stiffness:

$$k_i = \frac{F_{ni}}{\delta_i} = \frac{\Delta\tau_i}{P_{C_i}\Delta\theta_i r_i \cos(\varphi_i)} = \frac{\Delta\tau_i}{P_{C_i}\Delta\theta_i \sqrt{P_{C_i}^2 + h_i^2} \cos(\arctan(h_i/P_{C_i}))}. \quad (4)$$

By linear approximation, we take into account only two values of θ_i for τ_i nearest to 0.02 Nm and 0.05 Nm. Then, from the experimental diagrams (Fig. 5(a-e)) we obtain $\Delta\theta_i$ and $\Delta\tau_i$ and list them in Table 1.

TABLE I
FINDINGS FROM EXPERIMENTAL DIAGRAMS

Parameter	Sponge	Rubber sponge	Rubber	Wood
$\Delta\theta_i \cdot 10^{-4}$ [rad]	39.53	10.82	4.12	3.84
$\Delta\tau_i \cdot 10^{-2}$ [Nm]	2.98	3.0	2.79	2.92

The total elastic deformation δ_i is made up of elastic deformation caused by object compliance δ_o and one generated by joint flexibility δ_{ri} . That is, we can write:

$$\delta_i = \frac{F_{ni}}{k_i} = \delta_o + \delta_{ri} = \frac{R_{ni}}{k_o} + \frac{F_{ni}}{k_{ri}}, \quad (5)$$

where R_{ni} is the reaction, absolute value of which equals F_{ni} ; k_o and k_{ri} are stiffness of the object and stiffness of robot link, respectively.

The coefficient k_{ri} is mainly defined by torque sensor stiffness, harmonic drive stiffness, structural flexibility, and P-gain magnitude. Detailed examination has showed that complex theoretical model of robot link stiffness can hardly provide accurate estimation of k_{ri} . Therefore, we can set the value of robot link stiffness close to total stiffness in the most hard contact case. This assumption is valid because during impact with hard environment, such as aluminum plate, the contact deformation of the object is too small to be accounted for ($k_o \approx \infty$). Thus, using Eq. (2)-(4) and the data presented in Fig. 5(a-e) we derive unknown value of k_{ri} :

$$k_{ri} = \frac{0.0293 \text{ Nm}}{0.175 \cdot 2.758 \cdot 10^{-4} \cdot 0.1776 \cdot 0.986 \text{ m}^2} = 3468.6 \frac{\text{N}}{\text{m}}$$

The stiffness of the objects are calculated from the following equation:

$$k_o = \frac{k_{ri} \cdot k_i}{k_{ri} - k_i}, \quad (6)$$

where k_i is defined by Eq. (4). Derived values of k_i and k_o are given in Table 2.

TABLE II
TOTAL STIFFNESS AND OBJECT STIFFNESS

Parameter	Sponge	Rubber sponge	Rubber	Wood
k_i [N/m]	260.84	959.3	2343.78	2469.04
k_o [N/m]	282.04	1325.92	7223.94	8562.90

The obtained results demonstrate strong correspondence of correlation among calculated object stiffness with that of real objects. Naturally, the actual stiffness of colliding environment differs from calculated one with finite error. To achieve high accuracy, specific equipment is needed. However, our aim was only assessment of the danger level of robot arm collision with object. Specifically, we can define that sponge and rubber sponge material are safe for interaction, but rubber, wood, and metal pose threat while striking the robot arm. Consequently, we have succeeded in solving main task, that is, object classification by getting information about stiffness during impact.

In case when collision must be detected robustly without consideration of object properties, the value of time derivative of torque can be used to judge the impact value (Fig. 5(f)).

C. Shape Recognition and Contact Point Determination

The information about contact point coordinates is necessary in calculation of the object stiffness, applied force vector, and for shape reconstruction. The tactile sensor can be useful in this case. However, our goal is to perform tactile interaction with environment without complicated sensory system of the robot. The method, we are presenting here, results from the assumption that the coordinates of intersection of the subsequent profiles of the robot arm while tactile obstacle avoidance equals the coordinates of contact points. Since the increment of joint angles is small enough, we can detect contact point with admissible accuracy.

Let us consider the case when forearm is contacting with object. The line representing the robot forearm is located by the following position vectors:

$$P_t = \begin{bmatrix} P_{tx} \\ P_{ty} \\ P_{tz} \end{bmatrix} = \begin{bmatrix} L_2(s_1s_2s_3s_4 + c_1c_3s_4 + s_1c_2c_4) + L_1s_1c_2 \\ -L_2(c_2s_3s_4 - s_2c_4) + L_1s_2 \\ -L_2(c_1s_2s_3s_4 - s_1c_3s_4 + c_1c_2c_4) - L_1c_1c_2 \end{bmatrix} \quad (7)$$

$$P_e = \begin{bmatrix} P_{ex} \\ P_{ey} \\ P_{ez} \end{bmatrix} = \begin{bmatrix} L_1s_1c_2 \\ L_1s_2 \\ -L_1c_1c_2 \end{bmatrix} \quad (8)$$

where $s_1, s_2, s_3, s_4, c_1, c_2, c_3,$ and c_4 are abbreviations for $\sin(\theta_1), \sin(\theta_2), \sin(\theta_3), \sin(\theta_4), \cos(\theta_1), \cos(\theta_2), \cos(\theta_3),$ and $\cos(\theta_4)$, respectively; L_1, L_2 are the lengths of the upper arm and forearm, respectively, P_t, P_e are vectors locating tip of the robot and elbow joint, respectively.

On the next step of iteration $\theta_i + \Delta\theta_i$ we calculate the new coordinates of the end points of forearm. The intersection

point of two consequent lines will define the coordinates of contact point.

Object shape recognition is usually performed by global scanning. This method requires the sensor to scan large segments of an object surface that makes recognition process slow. We propose tactile object-recognition method based on the acquisition and formulation of information in the form of image primitives. Tactile images are generated when robot arm registers a series of contact points with an object. Graphical modelling of the movement of the robot arm following along round contour is shown in Fig. 7.

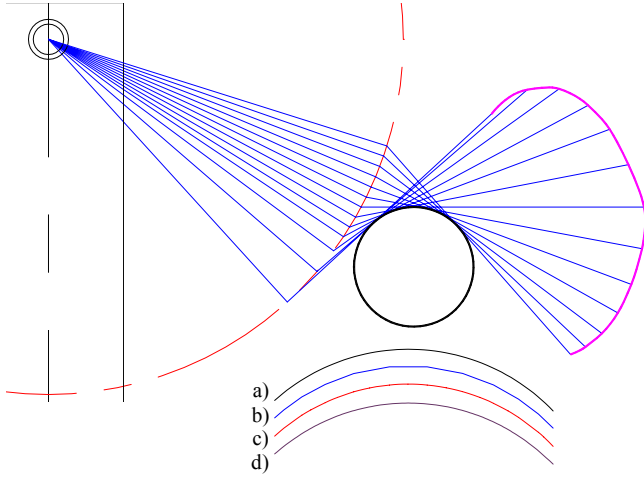


Fig. 7 Round shape recognition through tactile interaction

The node points obtained by employing the above-mentioned algorithm can be interpolated by B -splines [9]:

$$S_i(t) = \begin{bmatrix} t^2 & t & 1 \end{bmatrix} \frac{1}{2} \begin{bmatrix} 1 & -2 & 1 \\ -2 & 2 & 0 \\ 1 & 1 & 0 \end{bmatrix} \begin{bmatrix} p_{i-1} \\ p_i \\ p_{i+1} \end{bmatrix}, \quad (9)$$

where $S_i(t)$ is a quadratic parametric polynomial, p_i are the control points, $t \in [0,1]$ is the global parameter.

Fig. 7(a) shows arc of the object contour, while Fig. 7(b-d) represents polylines obtained by linear, arc, and B -spline interpolation (have precise convergence), respectively. The algorithm of following the contour of the rectangular-shaped object is as follows. In presence of vertex the lines intersect in one point. When coordinates of intersection point change drastically the edge of the object is recognized.

IV. CONTROL OF TACTILE INTERACTION OF ROBOT ARM WHILE OBSTACLE AVOIDANCE

To achieve skillful human-like behavior, the robot has to be able to change its dynamic characteristics depending on time-varying interaction forces. The most efficient method of controlling the interaction of a manipulator and environment is impedance control. This approach enables to regulate response properties of robot to external forces through modifying the mechanical impedance parameters [10].

The desired impedance properties of i -th joint of

manipulator can be expressed as:

$$J_{di}\Delta\ddot{\theta}_i + D_{di}\Delta\dot{\theta}_i + K_{di}\Delta\theta_i = \tau_{EXTi}; \quad \Delta\theta_i = \theta_{ci} - \theta_{di}, \quad (10)$$

where J_{di} , D_{di} , K_{di} are the desired inertia, damping, and stiffness of i -th joint, respectively; τ_{EXTi} is torque applied to i -th joint; $\Delta\theta_i$ is the difference between the current compliant angle θ_{ci} and desired one θ_{di} .

The state-space presentation of Eq. (10) is:

$$\begin{bmatrix} \Delta\dot{\theta}_i \\ \dot{v}_i \end{bmatrix} = \begin{bmatrix} 0 & 1 \\ -K_d/J_d & -D_d/J_d \end{bmatrix} \begin{bmatrix} \theta_i \\ v_i \end{bmatrix} + \begin{bmatrix} 0 \\ 1/J_d \end{bmatrix} \tau_{EXTi}(t), \quad (11)$$

where v_i is the state variable ($v_i = \Delta\dot{\theta}_i$).

The discrete presentation of Eq. (11) with sampling time of T is needed for program code implementation:

$$\begin{bmatrix} \Delta\theta_{k+1} \\ \Delta\dot{\theta}_{k+1} \end{bmatrix} = A_d \begin{bmatrix} \Delta\theta_k \\ \Delta\dot{\theta}_k \end{bmatrix} + B_d T_{EXT(k)}. \quad (12)$$

For the fastest non-oscillatory response we have:

$$A_d = e^{\lambda_1 T} \begin{bmatrix} 1 - \lambda_1 T & T \\ -K_d T / J_d & 1 - \lambda_1 T - D_d T / J_d \end{bmatrix}, \quad (13)$$

$$B_d = (A_d - I) A^{-1} B = \frac{1}{K_d} \begin{bmatrix} 1 - e^{\lambda_1 T} (1 - \lambda_1 T) \\ (D_d / (2J_d))^2 T e^{\lambda_1 T} \end{bmatrix}, \quad (14)$$

where I is the identity matrix.

The control algorithm includes several stages. When the joint torque value exceeds the threshold, the contact state is recognized. Then, the stiffness of the robot arm is assigned according to the calculated object stiffness. Finally, robot arm follows the trajectory of the object outline by means of local impedance controller. On each step of iteration the control system verifies the magnitude of the applied force vector to be equal constant value (Fig. 8).

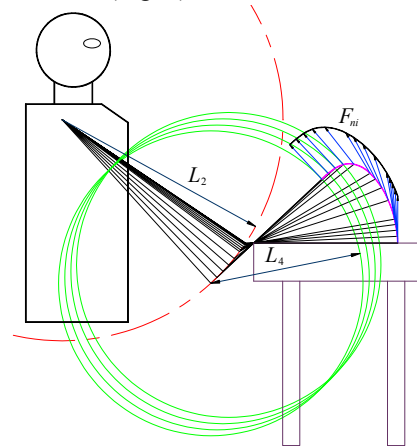


Fig. 8 Robot arm following the trajectory along the table surface

As example of control implementation, robot arm moving along the object surface is shown in Fig. 9.

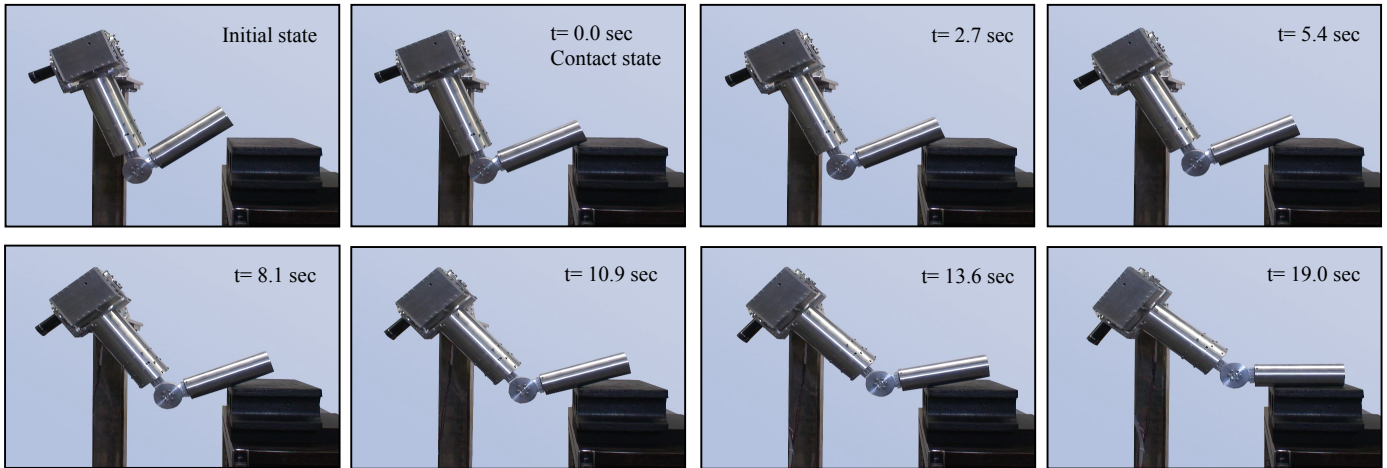


Fig. 9 Implementation of the obstacle avoidance through tactile interaction

The remarkable opportunity of ensuring safe robot-environment interaction is that we can establish different dynamic parameters of robot arm contacting with environment according to calculated object stiffness. This is inherent capability of humans, since when we collide with stiff objects we tend to soften our muscles as much as we can.

We summarize possible cases of application of the robot enabling intelligent tactile obstacle avoidance as follows:

- 1) In extremely cramped environment robot arm finds the path through interaction with obstacles.
- 2) A robot reaches for visible object located inside narrow space. The robot arm must contact and follow the surface of the obstacle represented by sides of the box to fulfill the task.
- 3) A robot reaches for object located beyond of the robot camera visibility range. In such cases robot arm needs to be equipped with additional cameras in order to process collision softly on its own.
- 4) A robot investigates the indoor area to achieve situational awareness without necessity of its bulky body to enter the room. When the situation is assessed, the robot body can elude the jamb and enter into the room carefully.
- 5) A robot structures the environment. A vision system of robots cannot determine the distance to the object in 3D space. By tactile interaction, robot can precisely define the object location and reachable working area.

V. CONCLUSIONS AND FUTURE WORK

In this paper we proposed a novel approach to obstacle avoidance through whole-arm tactile interaction. The developed robot arm and control system enable manipulator encountered with object to adapt the planned motion to the obstacle shape. Such algorithm is especially valuable for the real indoor environments, when obstacles change their location dynamically.

We proposed the methods of object stiffness evaluation, contact point calculation, and object shape reconstruction. To verify their feasibility and robustness, the experiments and simulations were performed. Obtained results show that many

essential parameters of the obstacle can be accurately identified through physical contact. The knowledge of object stiffness endows robot control with human-like ability to safely interact with environment. The robot can modify the joint compliance to avoid high impact forces.

Our future research will be devoted to control of the robot arm interacting with movable objects. The method of the friction estimation while pushing the object will also be the subject of our research.

ACKNOWLEDGMENT

The research is supported in part by a Japan Society for the Promotion of Science (JSPS) Postdoctoral Fellowship for Foreign Scholars.

REFERENCES

- [1] R. V. Mayorga, K. S. Ma, A. K. C. Wong, and B. Ressa, "A fast approach for the path planning of telerobotic manipulators," in *Proc. ICRA'93*, Vol. 2, 1993, pp. 289-294.
- [2] A. A. Maciejewski and C. A. Klein, "Obstacle avoidance for kinematically redundant manipulator in dynamically varying environment," *The Int. J. of Robotics research*, vol. 4, no.3 pp. 109-117, 1985.
- [3] V. J. Lumelsky, M. S. Shur, and S. Wagner, "Sensitive skin," *IEEE Sensors Journal*, Vol.1, No. 1, pp. 41-51, 2001.
- [4] V. Lumelsky and E. Cheung "Towards safe real-time robot teleoperation: automatic whole-sensitive arm collision avoidance frees the operator for global control," in *Proc. ICRA'91*, 1991, pp. 797-802.
- [5] A. M. Sabatini, V. Genovese, E. Guglielmelli, A. Mantuano, G. Ratti, and P. Dario, "A low-cost, composite sensor array combining ultrasonic and infrared proximity sensors," in *Proc. IROS'03*, 2003, pp. 120-126.
- [6] F. Caccavael, C. Natale, B. Siciliano, and L. Villani, "Six-DOF impedance control based on angle/axis representation," *IEEE Transaction on Robotics and Automation*, vol. 15, no. 2, pp. 289-300, April 1999.
- [7] J. Bauer, "Mobile robot with tactile arm used for exploration and pushing tasks," in *Proc. IROS'96*, 1996, pp. 560-567.
- [8] D. Tsetserukou, R. Tadakuma, H. Kajimoto, and S. Tachi, "Optical torque sensors for implementation of local impedance control of the arm of humanoid robot", in *Proc. ICRA'06*, 2006, pp. 1674-1679.
- [9] F. Yamaguchi, *Curves and Surfaces in Computer Aided Geometric Design*. Berlin, Germany: Springer-Verlag, 1988.
- [10] N. Hogan, "Impedance control: an approach to manipulation, Part I-III," *ASME Journal of Dynamic Systems, Measurement and Control* vol. 107, pp. 1-23, March 1985.